

ENSO influences on Southern Hemisphere column ozone during the winter to spring transition

M. H. Hitchman¹ and M. J. Rogal¹

Received 17 July 2009; revised 21 June 2010; accepted 22 June 2010; published 20 October 2010.

[1] This study investigates how the El Niño Southern Oscillation (ENSO) modulates the distribution of column ozone during the Southern Hemisphere (SH) winter to spring transition, when a zonal asymmetry in column ozone develops near 55°S, with a maximum south of Australia. ENSO differences in column ozone and planetary wave structure are explored for the average of seven El Niño (EN) versus six La Niña (LN) events during 1982–2004. A westward shift in convection during LN corresponds to a 30–50° westward shift of SH planetary wave and column ozone patterns. The extratropical lower stratospheric temperature anomalies are inversely correlated with tropical anomalies in similar longitude bands and are highly correlated with local column ozone anomalies. The tropical signal is communicated to higher latitudes by modulating subtropical anticyclones, with distinctive responses for EN and LN years for each month. During August and EN a subtropical anticyclone extends from South America to South Africa, and the wave one asymmetry of the Antarctic vortex is more pronounced and shifted eastward, along with column ozone. In September and EN a strong anticyclone exists over South Africa, with a corresponding cold, ozone-poor anomaly in the stratosphere, diminishing the western edge of the ozone maximum. In October and LN a strong anticyclone exists over Australia, with an amplified trough on its poleward flank. This trough is overlain by an ozone-rich warm anomaly, which expands the western edge of the ozone maximum, and the polar vortex asymmetry is amplified and rotated westward.

Citation: Hitchman, M. H., and M. J. Rogal (2010), ENSO influences on Southern Hemisphere column ozone during the winter to spring transition, *J. Geophys. Res.*, 115, D20104, doi:10.1029/2009JD012844.

1. Introduction

[2] The global distribution of column ozone is strongly influenced by short-term and long-term variability in meteorological fields. The position of the time mean maximum in total ozone is highly correlated with the region of the maximum mean baroclinicity and the Southern Hemisphere (SH) storm track near 50–60°S [Berbery and Vera, 1996]. Strong correlations exist between column ozone and tropopause height [Schubert and Munteanu, 1988; Steinbrecht *et al.*, 1998], lower stratospheric temperature anomalies [Labitzke and van Loon, 1992] and lower stratospheric potential vorticity anomalies [Hood *et al.*, 1999]. During SH winter ozone is distributed in a collar shape [e.g., Stolarski *et al.*, 1990; Randel *et al.*, 2002], just poleward of the subtropical westerly jet. During SH spring a distinctive ozone maximum amplifies south of Australia, creating an “ozone croissant” shape in polar stereographic projection. The fundamental wave-one nature of the SH

lower stratospheric temperature and ozone anomaly has been noted in previous work [Newman and Randel, 1988; Wirth, 1991, 1993; Quintanar and Mechoso, 1995a, 1995b; Hio and Hirota, 2002]. Hitchman and Rogal [2010] showed that the eastward migration of Southeast Asian convection from August to October is related to an eastward shift in the location of the ozone maximum, with changes in convective outflow influencing the SH longwave pattern and ozone via modulation of subtropical anticyclones and the subtropical westerly jet structure in the upper troposphere and lower stratosphere (UTLS).

[3] Bojkov [1987] analyzed Total Ozone Mapping Spectrometer (TOMS) data and suggested that the eastward shift in the column ozone maximum in the SH midlatitudes during the 1983 El Niño (EN) event relative to the 1985 La Niña (LN) event was related to an eastward shift in tropical convection. Shiotani [1992] studied the effects of ENSO on tropical column ozone during 1979–1989. Tropical zonal mean changes were on the order of 6 DU, with less during EN events. He also found an east-west tropical dipole in column ozone, with more ozone over Indonesia during EN and more over the Eastern Pacific during LN, with amplitude ~6 DU. Kayano [1997] analyzed TOMS data for the 12 year period 1979–1991, using empirical orthogonal functions with a low-pass filter which eliminated variability

¹Department of Atmospheric and Oceanic Sciences, University of Wisconsin–Madison, Madison, Wisconsin, USA.

at time scales of less than about a year. An antiphased ENSO dipole in column ozone in the SH midlatitudes relative to the tropical dipole was confirmed in this data record, with a westward shift in the midlatitude ozone maximum during LN. *Kayano* [1997] found that the ENSO signal in midlatitude total ozone was highly correlated with lower stratospheric temperatures. Here we show monthly mean composites of TOMS data over the 22 year record 1982–2004, with a focus on month to month changes in ENSO differences during August–September–October (ASO), when the ozone croissant is present.

[4] During the period 1982–2004, ENSO and the stratospheric quasi-biennial oscillation (QBO) were moderately correlated for ASO means. In this 22 year sample, QBO westerly shear in the layer 30–50 hPa coincided with 5 out of 7 ENs, while QBO easterly shear coincided with 5 out of 6 LNs. This makes it difficult to cleanly establish causal attribution to ENSO, since both ENSO and the QBO affect polar stratospheric planetary waves, winds, and temperatures [e.g., *van Loon et al.*, 1982; *van Loon and Labitzke*, 1987; *Hamilton*, 1993]. QBO effects on ozone have been documented by *Hasebe* [1980], *Bowman* [1989], *Stolarski et al.* [1991], *Angell* [1992], *Shiotani* [1992], and *Randel and Cobb* [1994]. In the tropics there is ~8 DU less ozone when QBO easterly shear is in the lower stratosphere compared to QBO westerly shear, due to an elevated tropopause and enhanced upwelling. Middle stratospheric QBO wind regimes influence extratropical planetary wave behavior (and ozone) in the SH springtime [*McCormack and Hood*, 1994; *Baldwin and Dunkerton*, 1998; *Kinnersley and Tung*, 1998, 1999; *Pascoe et al.*, 2005; *Hampson and Haynes*, 2006; *Hitchman and Huesmann*, 2009]. However, modeling studies [e.g., *Sassi et al.*, 2004; *Garcia-Herrera et al.*, 2006] show significant differences in temperatures in the polar stratosphere between EN and LN events with no QBO. In addition, *Garfinkel and Hartmann* [2007] showed that the ENSO-QBO relationship has changed over time, with a correlation of -0.25 during 1957–1982 but during 1990–2007 the correlation was +0.26, even though the correlation was close to zero for their full 50 year record. It is important to note that the QBO may have contributed to differences between the “LN” and “EN” averages.

[5] The monthly evolution of the influence of ENSO on column ozone and dynamical fields is explored in detail during the SH winter to spring transition, when the ozone croissant reaches its maximum. Data and significance tests are described in section 2. In section 3 the variation of column ozone with ENSO and month is described. The westward shift in column ozone and tropical convection during LN relative to EN are shown. In section 4 different mechanisms responsible for the eastward shift during EN and westward shift during LN are highlighted in separate subsections for August, September, and October. It is found that ENSO exerts its influence on extratropical column ozone via longitudinal shifts in convective outflow and associated modulation of subtropical high pressure systems in the UTLS. Longitude-altitude sections of height and temperature anomalies illustrate the continuous tropical-to-polar connection of the planetary wave pattern. A distinct westward shift in the ozone croissant and westward rotation of the polar vortex accompanies the westward shift in convection during LN. Dynamical mechanisms

underlying this relationship are described in section 5, followed by conclusions.

2. Data and Methodology

[6] The TOMS column ozone data set used in our study encompasses the period 1982–2004, including data from the following spacecraft: Nimbus 7 (11/1/1978–5/6/1993), Meteor 3 (8/22/1991–11/24/1994), and Earth Probe (7/22/1996–12/14/2005) (<http://toms.gsfc.nasa.gov>). We have limited analysis to the August–September–October (ASO) period to focus on the SH late winter to early spring transition. The ASO period for 1995 is unavailable for analysis, yielding 22 ASO periods during 1982–2004.

[7] Monthly mean meteorological data fields were derived from 2.5° gridded European Centre for Medium Range Weather Forecasts (ECMWF) global upper air analyses [*Trenberth*, 1992; *Hollingsworth et al.*, 1986; *Kallberg et al.*, 2005]. The period 1995–2004 was used in this study.

[8] In order to analyze the interactions between ENSO and column ozone we created subsets of data using the Oceanic Nino Index (ONI), available from the National Oceanic and Atmospheric Administration Climate Prediction Center, to identify cold and warm events (<http://www.cpc.noaa.gov>). The ONI index, which is based on a 3-month running mean of sea surface temperature anomalies in the NINO 3.4 region (5°S to 5°N, 120–170°W), is the core of the Multivariate ENSO Index (MEI), which is widely used in similar analyses. Correlations between the ONI and MEI indices are 0.93, 0.98, and 0.98 for August, September, and October, respectively, supporting our decision to use the ONI. We assumed an index threshold value of ±0.4, which produced seven ASO EN periods (1982, 1986, 1987, 1991, 1997, 2002, 2004) and six ASO LN periods (1983, 1984, 1988, 1998, 1999, 2000). It should be noted that ASO 1983 is categorized as strong LN using the ONI index but as a waning, weak EN using the MEI index. These LN and EN events are fairly evenly distributed between the first and second half of the data records.

[9] Of central interest is to determine the statistical significance of differences between column ozone, height, and temperature patterns among August, September, and October and between LN and EN. Student’s T-statistic

$$T = \frac{X - Y}{\sqrt{\sigma_X^2/N + \sigma_Y^2/M}} \quad (1)$$

is used to assess the probability that two sample populations have meaningfully distinct averages, X and Y , with variances σ_X^2 and σ_Y^2 , and degrees of freedom N and M . For ENSO differences the number of degrees of freedom are taken as $N = 6$ La Ninas and $M = 7$ El Ninos for TOMS and $N = 3$ and $M = 3$ for the 1995–2004 ECMWF record. For interannual differences among ASO $N = M = 22$, corresponding to the number of ASO seasons used in the TOMS record, while $N = M = 10$ for the ECMWF record. Patterns of ENSO differences in column ozone are very similar for the periods 1982–2004 and 1995–2004. The longer record was used for column ozone results shown here.

[10] Maps of standard deviation and statistical significance for differences between monthly means are described by *Hitchman and Rogal* [2010], who showed that there is a

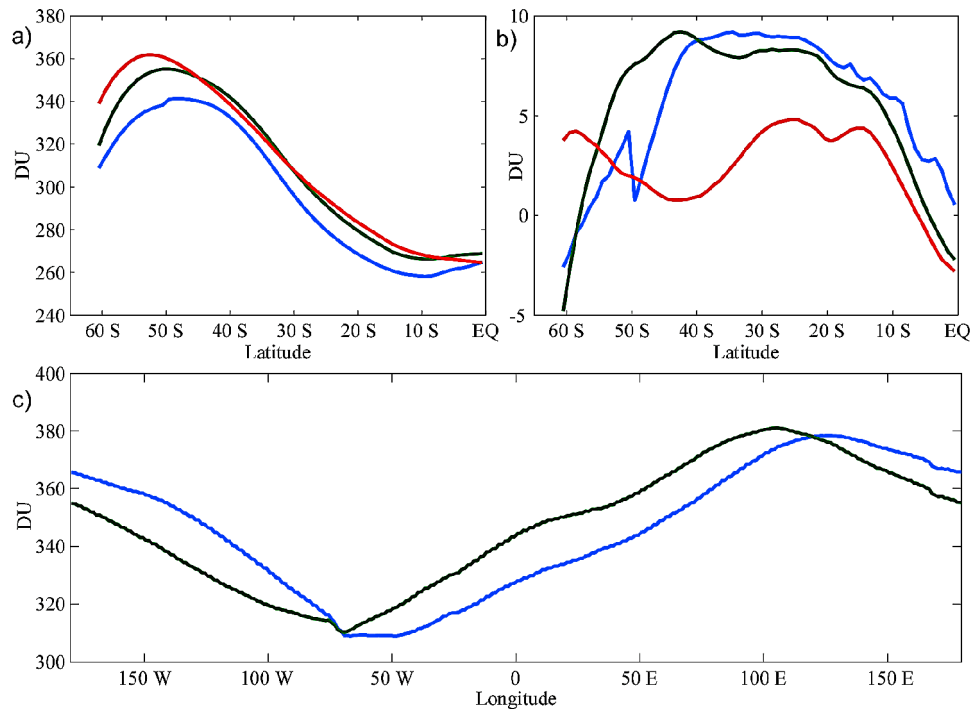


Figure 1. Zonally averaged (a) TOMS column ozone during 1982–2004 and (b) differences between La Nina and El Nino conditions in the Southern Hemisphere for August (blue), September (green), and October (red), and (c) the longitudinal variation of column ozone averaged in the 45°–60°S band during August–October for La Nina (green) and El Nino (blue) events. Note the seasonal increase at high latitudes in Figure 1a, greater hemispheric ozone content during La Nina in Figure 1b, and a 30–50° westward shift of the high-latitude ozone asymmetry during La Nina in Figure 1c.

seasonal eastward shift and intensification of the column ozone maximum from August to October, with differences between monthly means significant at the 99% level. The westward shift in the ozone maximum for LN relative to EN in each month is also significant at the 99% level, as shown in the right-hand column of Figure S1 in the auxiliary material.¹ Standard deviations in the midlatitudes and especially in the ozone maximum are larger during LN for all 3 months (Figure S1). Figures S2–S4 show that ENSO differences in temperature and geopotential height anomalies associated with the westward shift in ozone are also quite significant even though only three El Nino and three La Nina events were included.

3. ENSO Modulation of Tropical Temperatures and Zonal Mean Column Ozone

[11] Zonal mean column ozone for the ASO period varies in a sinusoidal fashion with latitude (Figure 1a), exhibiting a minimum of 260–270 DU just south of the equator, a maximum of ~350 DU around 50°S, then diminishing into the Southern Polar Vortex (SPV). Extratropical column ozone increases with time from austral winter to early spring, with maximum values in October at 55°S ~20 DU higher than in August. Ozone is produced in the sunlit

tropical middle stratosphere and is then transported via planetary and synoptic waves toward higher latitudes. The ozone minimum near 10°S in the austral winter is due to a combination of a high tropical tropopause plus reduced photochemical production relative to the summer subtropics [Perliski *et al.*, 1989]. Planetary and synoptic waves reaching into the subtropical stratosphere transport ozone poleward and downward, where ozone gradually accumulates in the surf zone poleward of the subtropical westerly jet and equatorward of the polar night jet [Hudson *et al.*, 2003, 2006; Hitchman and Rogal, 2010]. Column ozone increases as winter transitions into early spring and wave activity increases, enabling more ozone to be transported southward and downward from its production regions. During the ASO period the hemispheric average column ozone (0–60°S) increases by ~13 DU, with ~20 DU increase near 55°S (Figure 1a).

[12] The differences found in column ozone between LN and EN generally do not exceed 5% of the average column ozone values for a given latitudinal band but are nevertheless pronounced (Figure 1b). LN periods tend to have higher ozone content than EN events. Zonal mean differences are greatest in August and September, when column ozone is 5–10 DU higher in the band 10–55°S (Figure 1b).

[13] In the band 45–60°S (Figure 1c) ASO average column ozone exhibits a wave one pattern with a maximum of ~380 DU near 110°E and a minimum of ~310 DU near 70°W, for a range of 70 DU. During LN this entire pattern is shifted westward by 30–50°, yielding increases in column ozone of ~20 DU from 70°W eastward to 100°E during LN

¹Auxiliary materials are available in the HTML. doi:10.1029/2009JD012844.

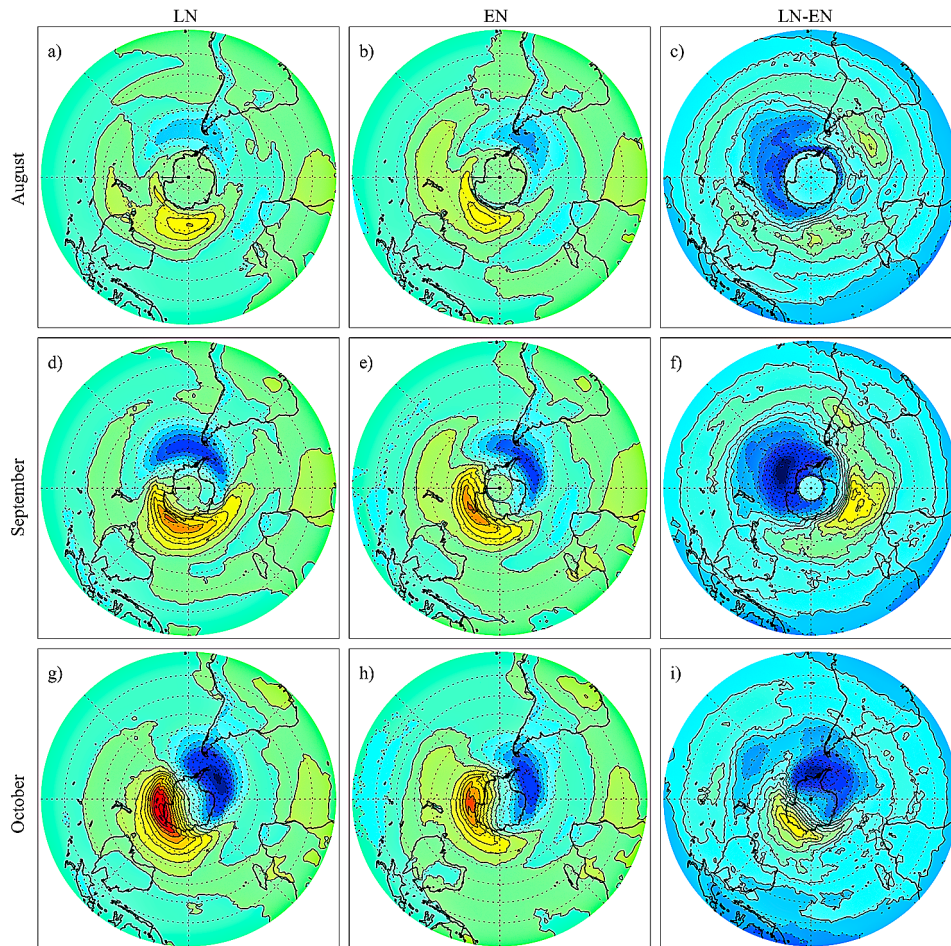


Figure 2. Southern Hemisphere TOMS column ozone departures from the zonal mean for (a) August LN, (b) August EN, (c) August LN-EN, (d) September LN, (e) September EN, (f) September LN-EN, (g) October LN, (h) October EN, and (i) October LN-EN. The contour interval is 15 DU for LN and EN means and 5 DU for LN-EN differences. Low values are highlighted in blue while high values are highlighted in yellow and orange. Note the westward shift in the high-latitude ozone pattern during LN relative to EN in each month.

and increases of ~ 20 DU from 130°E eastward to 70°W during EN.

[14] Figure 2 shows the progression of column ozone anomalies from August to October (top to bottom) during LN (left), EN (middle), and the LN-EN differences (right). There is a seasonal eastward progression and amplification of the midlatitude ozone maximum from August to October [Hitchman and Rogal, 2010] that is seen for both the LN and EN composites. However, for each month the ozone maximum is displaced westward during LN relative to EN (compare left and center). Tropical column ozone exhibits a relative minimum over Indonesia during LN, consistent with a colder, higher tropopause [cf. Shiotani, 1992]. During EN there is more column ozone at the eastern end of the ozone maximum, over the high-latitude Central and Eastern Pacific, while during LN there is more column ozone at the western end of the ozone maximum, over the high-latitude Southern Indian Ocean.

[15] Differences between LN and EN (Figures 2c, 2f, and 2i) exhibit interesting geographical patterns that are

distinct for each month. During September there is a striking LN-EN column ozone maximum south of South Africa (Figure 2f). During October this pattern rotates eastward, with a pronounced LN-EN column ozone maximum south of Australia (Figure 2i). Column ozone differences are quite significant in these two geographical locations, exceeding 30 DU. Column ozone in the SPV is reduced by up to 45 DU during LN.

[16] The westward shift in tropical convection during LN is shown in Figure 3, as seen in changes in the planetary-scale temperature patterns in the tropics. During LN the midtroposphere is anomalously warm from Indonesia into the Pacific and is anomalously cold from the Atlantic to Africa, while the tropopause anomalies are the reverse, forming a planetary-scale quadrupole pattern. During EN this pattern diminishes from August to October. The cold pool at 100 hPa over Indonesia and the Western Pacific is more pronounced and located farther westward during LN for each month (Figure 3). The differences between LN and EN near 120°E are striking. The strong cold pool in the

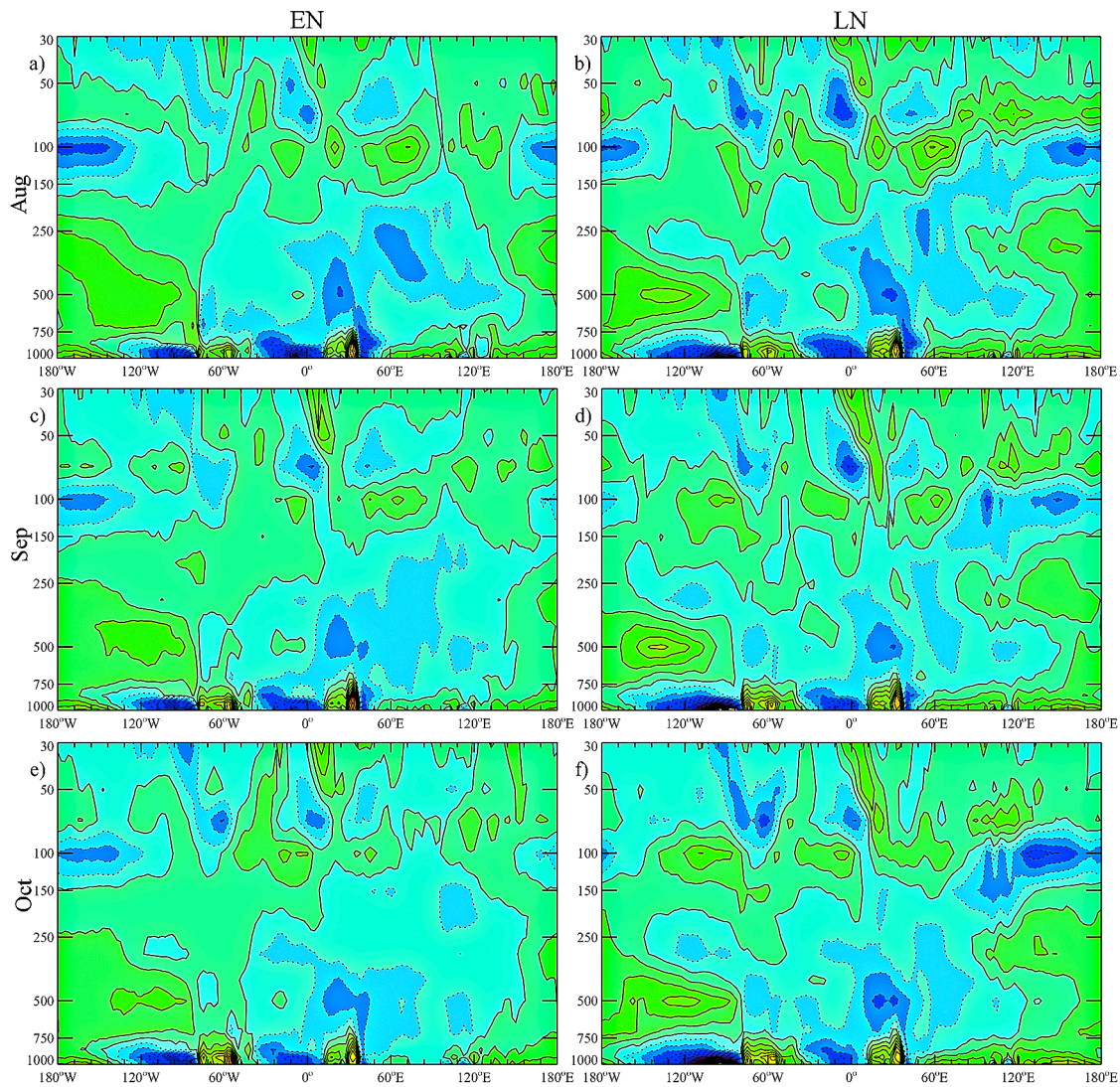


Figure 3. Longitude-altitude sections at the equator of ECMWF temperature departures from the zonal mean during 1995–2004 for (a) August EN, (b) August LN, (c) September EN, (d) September LN, (e) October EN, and (f) October LN. The contour interval is 1 K, with warm (cool) anomalies highlighted with solid contours and light green (dashed contours and dark blue). Note the westward shift of the lower stratospheric cold anomaly centered near Indonesia during LN.

UTLS over Indonesia is notable during October in the LN composite (Figure 3f).

4. ENSO Differences in Geopotential Heights and Temperatures

[17] We now examine LN-EN differences in geopotential height and temperature to explore the dynamical nature of the midlatitude differences in column ozone separately for August, September, and October. Polar stereographic charts of 150 hPa Z' , 100 hPa T' , and 50 hPa T' are discussed and compared with longitude-altitude sections of Z' and T' at 20°S, 35°S, and 57.5°S for each month. Here 50 hPa Z' is not shown since it is similar to the 100 and 50 hPa T' patterns.

[18] In general, extratropical column ozone anomalies are more readily related to temperature anomalies than to height anomalies, due to the relationship between sub-

sidence warming and downward advection of ozone in the lower stratosphere. It will be shown that subtropical UTLS anticyclones are bracketed above and below by cold and warm anomalies. A lower stratospheric temperature anomaly that exists in a certain longitude band in the tropics is accompanied by an extratropical lower stratospheric temperature anomaly of the opposite sign, in the same longitude band.

[19] During August in the EN composite an anomalous UTLS anticyclone stretching from South Africa to South America coincides with amplification and an eastward shift of the extratropical planetary wave pattern and column ozone distribution. During September in the EN composite an anomalous UTLS anticyclone exists off the tip of South Africa, coinciding with a colder stratospheric anomaly above it and reduced column ozone at the west end of the ozone maximum. During October in the LN composite an anoma-

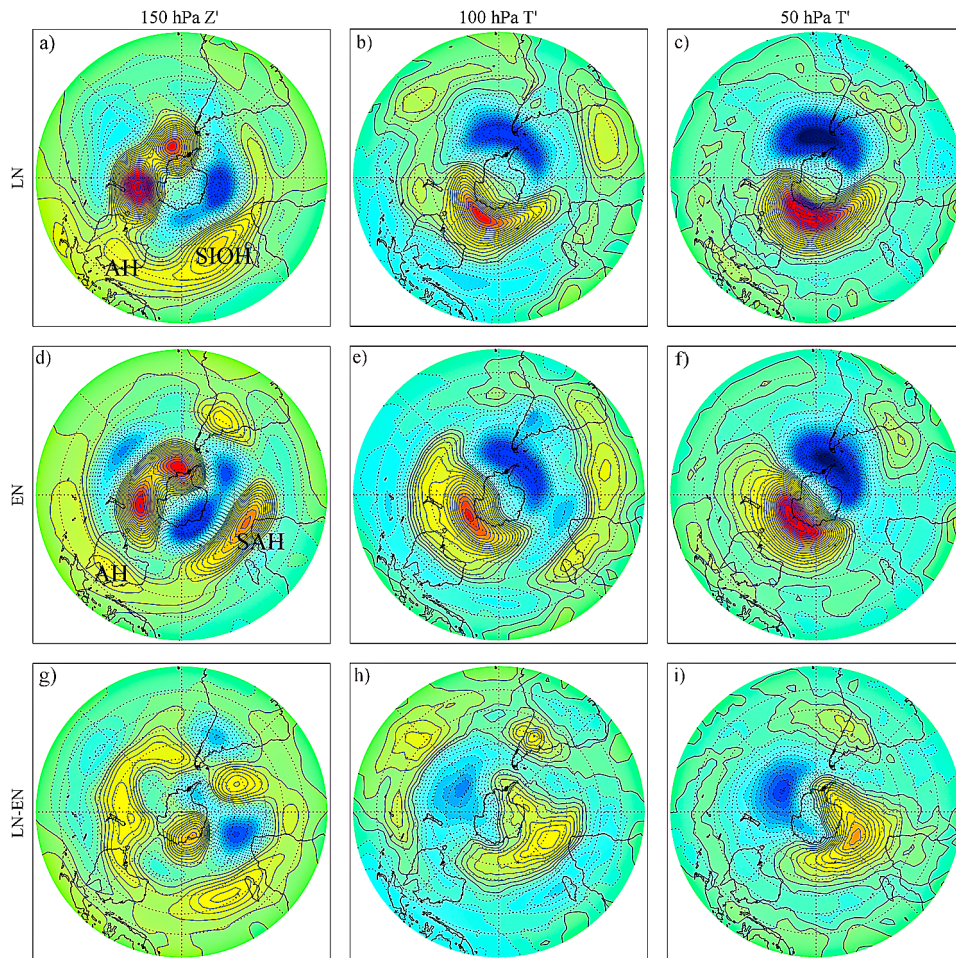


Figure 4. Planetary wave patterns during August for LN (a) 150 hPa Z' , (b) 100 hPa T' , (c) 50 hPa T' , for EN (d) 150 hPa Z' , (e) 100 hPa T' , (f) 50 hPa T' , and for LN-EN differences of (g) 150 hPa Z' , (h) 100 hPa T' , and (i) 50 hPa T' . The contour interval is 10 m for Z' and 1 K for T' . Low (high) values are highlighted in blue (red). The South African High (SAH) and Australian High (AH) are indicated. Note the extension of the SAH from Africa to South America in Figure 4d and the amplified wave one pattern in high latitudes in Figures 4e and 4f during EN.

lous UTLS anticyclone exists over Australia, coinciding with an amplified trough on its poleward flank, with an ozone-rich warm air mass adding to the western end of the ozone maximum. Inspection of Figures S1–S4 shows that LN-EN differences in each of these subtropical UTLS anticyclones and extratropical thermal and ozone anomalies are significant above the 97.5% level.

4.1. August

[20] At 150 hPa during August an anticyclone exists near 20°S over Australia, immediately poleward of intense Indonesian convection (Figures 4a and 4d). This Australian High (AH) stretches southwestward across the Southern Indian Ocean toward the tip of South Africa near 35°S, where a second maximum is found. During LN there is a distinct Southern Indian Ocean High (SIOH; Figure 4a), while during EN there is a distinct South African High (SAH; Figure 4d). During EN the SAH extends further southwestward across the Atlantic to the southern tip of South America, forming a South American High (SAMH;

Figure 4d). Poleward of the South African High is a trough, as part of a wave-one pattern in Z' , which is more pronounced during EN (Figures 4a and 4d).

[21] The subtropical anticyclone system is topped by colder air at 100 hPa as part of a wave-one pattern, with warmer air being found south of Australia and over the high-latitude Pacific (Figures 4b and 4e). This thermal structure extends well into the stratosphere (Figures 4c and 4f), with amplification of the warm anomaly south of Australia and of the cold anomaly near the Weddell Sea. Note that the barotropic warm (cold) anomaly coincides closely with the ozone maximum (minimum) in Figure 2. This wave-one pattern is amplified and rotated ~30° eastward during EN (Figures 4e and 4f) relative to LN (Figures 4b and 4c). In the LN-EN difference plots for T' (Figures 4h and 4i), the enhanced warm anomaly during EN is seen as a negative region south of Australia and the enhanced cold anomaly during EN over the South Atlantic is seen as a positive anomaly. The eastward shift of the warm anomaly

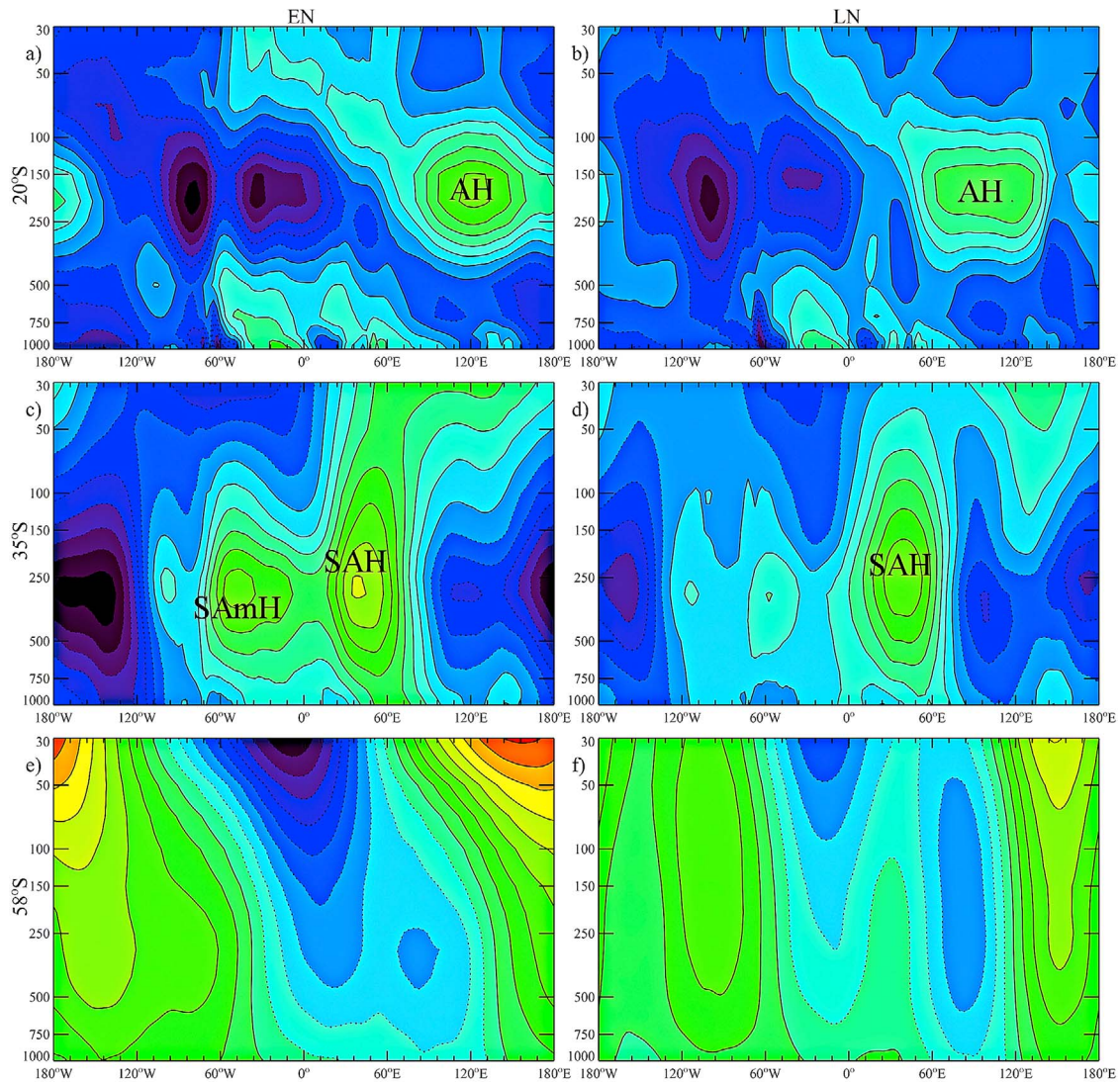


Figure 5. Longitude-altitude sections of August geopotential height anomalies during (a) EN at 20°S, (b) LN at 20°S, (c) EN at 35°S, (d) LN at 35°S, (e) EN at 57.5°S, and (f) LN events at 57.5°S. The contour interval is 10 gpm in Figures 5a and 5b, 20 gpm in Figures 5c and 5d, and 50 gpm in Figures 5e and 5f. Values range from low (dark blue) to high (yellow and red). The Australian High (AH), South African High (SAH), and South American High (SAMH) are indicated. Note the extended SAMH-SAH complex in Figure 5c and amplified wave one in Figure 5e during EN.

during EN yields a negative anomaly over the Pacific in the LN-EN column ozone difference (Figure 2c).

[22] Differences in planetary-scale structures in Z' and T' for August are shown in Figures 5 and 6. The subtropical SH UTLS region is dominated by a wave 1 structure with a positive anomaly located between 500 hPa and 70 hPa over Australia for both ENSO phases (Figures 5a and 5b). August height anomalies at 20°S display an increased amplitude during EN (Figure 5a) in comparison to those during LN (Figure 5b). A distinct westward shift is visible during LN relative to EN, consistent with the westward shift in convection. Near 35°S a deep anticyclonic anomaly is seen over South Africa in both LN and EN, with a pronounced westward extension to a South American High during EN (Figures 5c and 5d). This wave-one pattern in the UTLS at

35°S is nearly out of phase relative to 20°S. In comparison to EN, the Z' pattern for LN at 35°S has a smaller wave-one amplitude. This difference in amplitude is also seen at 57.5°S (Figures 5e and 5f). During EN a larger-amplitude baroclinic wave-one structure dominates, with the midstratospheric trough located near 0°E, while during LN the height anomalies are more barotropic and a wave-three component is more evident. During LN there are three anticyclonic structures: near 100°W, 50°E, and 150°E, confirming the wave-three LN-EN difference pattern in Figure 4g.

[23] Temperature anomalies at 20°S (Figures 6a and 6b) in the UTLS are smoother and displaced westward some 60° of longitude relative to the pattern seen at the equator (Figure 3). The temperature structure exhibits a wave-one quadrupole pattern, with a cold anomaly in the lower

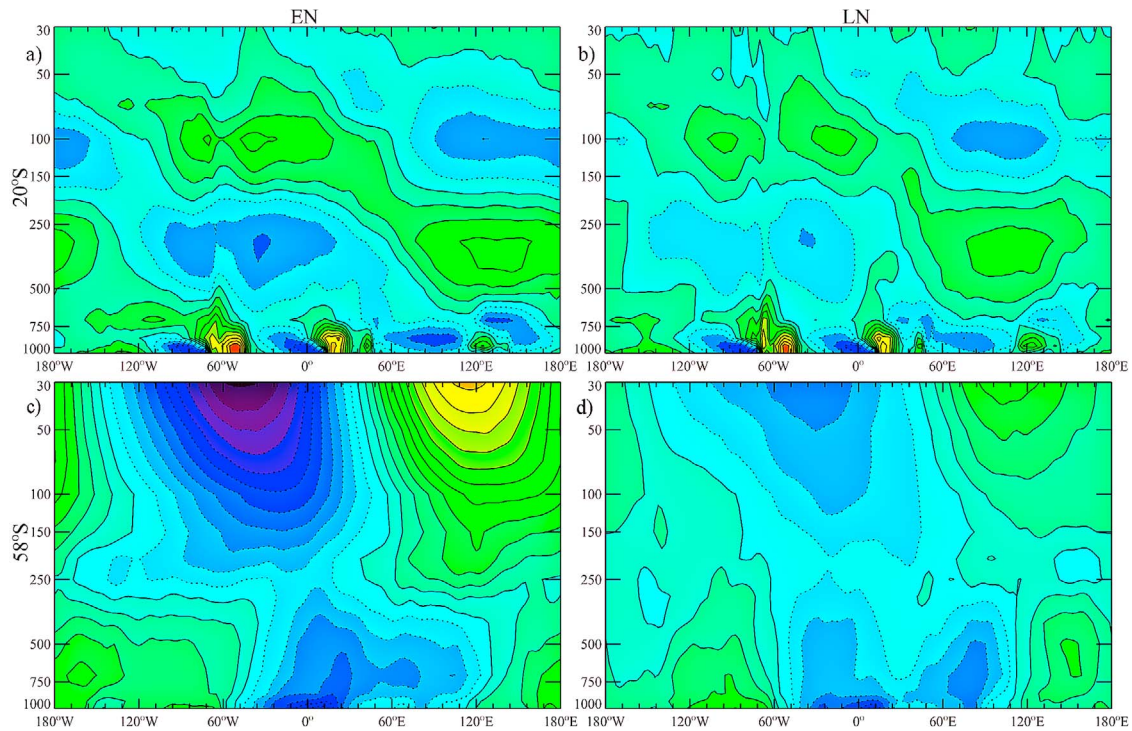


Figure 6. As in Figure 5, except for temperature anomalies, with contour interval 1 K. Note the anti-phased relationship between subtropical and extratropical temperature anomalies in the lower stratosphere.

stratosphere overlying midtropospheric warm air centered over Indonesia and a warm anomaly in the lower stratosphere overlying midtropospheric cold air centered over the Atlantic. The pattern is clearly amplified in the EN composite. A comparison with height anomalies in Figures 5a and 5b shows that a subtropical anticyclone in the UTLS overlies a warm tropospheric anomaly and underlies a cold stratospheric anomaly, consistent with hydrostatic thickness arguments.

[24] The wave-one T' structure above ~ 250 hPa apparent at 20°S is evident at 57.5°S in the same longitude bands, but with the opposite sign (Figures 6c and 6d), and the stronger EN pattern is also evident at both latitudes during August. The magnitude of the high latitude warm anomaly in August is 10 K larger during EN than during LN. Similarly, the negative anomaly region is 14 K colder during EN conditions.

4.2. September

[25] In September the two primary features in LN-EN differences in column ozone are the maximum off the tip of South Africa and minimum over the high-latitude Southeastern Pacific (Figure 2f). During September the height anomalies in the subtropical UTLS are somewhat different than in August. During LN a subtropical anticyclone is centered over the Southern Indian Ocean, the Southern Indian Ocean High (SIOH) (Figure 7a), while during EN a strong anticyclone is found near the tip of South Africa (Figure 7d). This results in substantial LN-EN differences in the subtropics at 150 hPa (Figure 7g). The strengthened anticyclone over South Africa during EN is consistent with enhanced rainfall over Central and Southern Africa in SH

spring during September and October when rainfall is diminished over Indonesia [see *Hastenrath*, 1990, Figure 3e].

[26] Above the strong South African High during EN lies anomalously cold stratospheric air (Figures 7e and 7f), consistent with reduced column ozone, which coincides very well with the LN-EN positive column ozone anomaly in Figure 2f. This LN-EN ozone anomaly may therefore be interpreted as a reduction in column ozone south of South Africa during EN. The entire long-wave pattern for EN is also rotated eastward relative to LN (compare Figures 7b and 7e and Figures 7c and 7f), leading to a warm anomaly and more column ozone over the high-latitude Southeastern Pacific during EN, thereby accounting for the negative LN-EN temperature anomaly (Figures 7h and 7i) and negative column ozone anomaly (Figure 2f) in this region.

[27] In September, height anomalies at 20°S are smaller than in August for both EN and LN conditions (Figures 8a and 8b). At 35°S (Figures 8c and 8d) there is a notable enhancement of the anticyclone near the tip of South Africa, which is much more pronounced during EN. This height anomaly over South Africa raises the tropopause and circulates low-ozone tropical UTLS air into the region, causing a reduction in ozone during EN (Figure 2e). This UTLS positive anomaly is coupled with a wave 1 ridge in the middle stratosphere. This vertical coupling for LN during September is much more effective than during August (compare Figures 8d and 5d). This midstratospheric (~ 30 hPa) wave 1 pattern extends from 35°S to 57.5°S .

[28] Near 57.5°S during September a wave-one structure dominates for both LN and EN (Figures 8e and 8f). The structure for EN is less organized than it was during August (Figures 8e and 5e), but the LN structure is radically

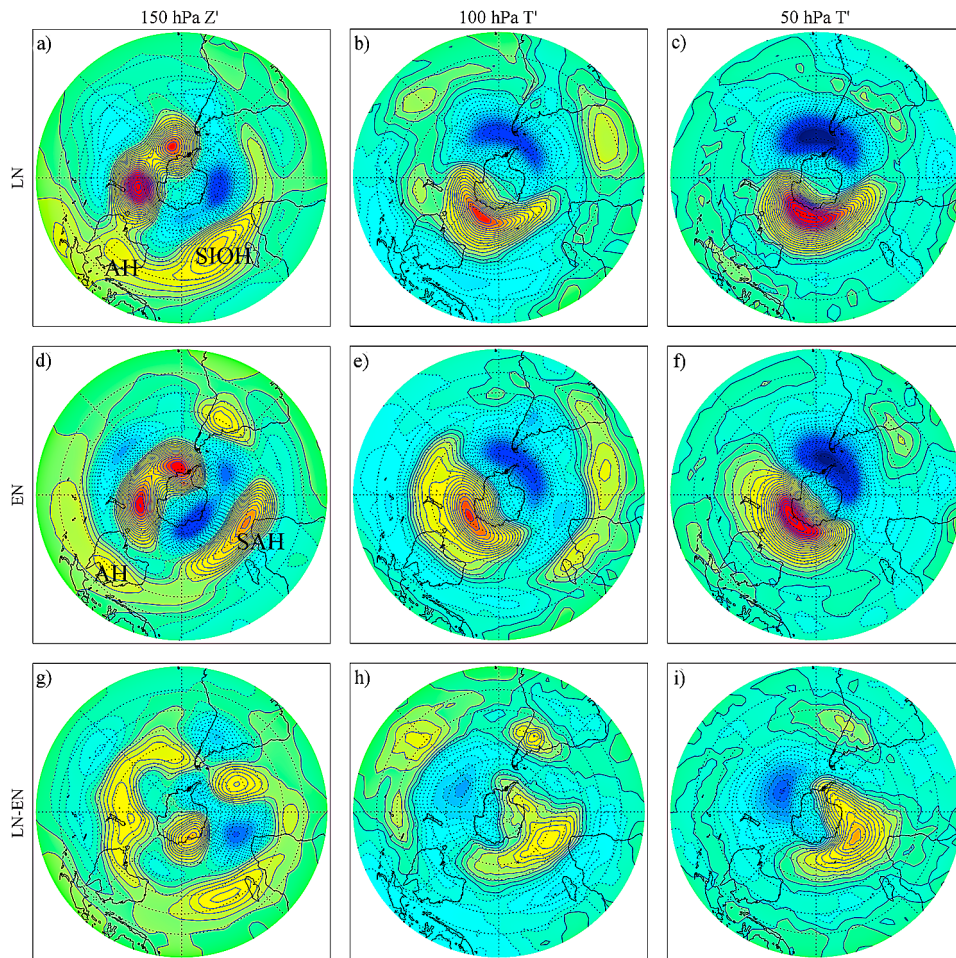


Figure 7. As in Figure 4, except for September. The Australian High (AH), Southern Indian Ocean High (SIOH), and South African High (SAH) are indicated. Note the SAH in Figure 7d and associated cold feature in Figures 7e and 7f during EN, resulting in an eastward rotation of the planetary wave pattern.

different in September, with a large amplitude, westward tilting ridge and trough pair (Figures 8f and 5f). The overall result is a wave one pattern that is comparable in amplitude for LN and EN but exhibits slightly greater westward tilt with height during LN. Corresponding sections of T' are not shown for September, but they also conform to the spatial paradigm of antiphased planetary wave temperature structures in the tropics and extratropics for given longitude bands in the lower stratosphere.

4.3. October

[29] In October the primary LN-EN features in column ozone are the maximum south of Australia and minimum near the Weddell Sea. (Figure 2i). This pattern is rotated $\sim 90^\circ\text{E}$ eastward relative to September (Figure 2f). At 150 hPa, LN favors a stronger UTLS anticyclone over Australia (Figure 9a), while EN favors a stronger UTLS anticyclone over South Africa, which extends toward South America (Figure 9d). The difference plot (Figure 9g) shows a pronounced geopotential height maximum during LN stretching from Australia to Madagascar, with a negative 150 hPa height anomaly on its poleward flank, south of Australia.

This 150 hPa trough coincides with the maximum in LN-EN differences in column ozone (Figure 2i).

[30] Again, during October, the link between temperature and column ozone anomalies is quite clear. The barotropic temperature maximum south of Australia is warmer and rotated toward the west during LN relative to EN (compare Figures 9b and 9c and Figures 9e and 9f). LN-EN temperature differences (Figures 9h and 9i) show a strong temperature maximum south of Australia, which coincides with the LN-EN maximum in column ozone (Figure 2i). The LN-EN temperature minimum near the Weddell Sea (Figures 9h and 9i) coincides with the LN-EN minimum in column ozone (Figure 2i). Two significant aspects of the planetary wave structure during October which relate to this barotropic warm anomaly during LN include the amplified subtropical UTLS anticyclone near Australia during LN (Figure 9a) and the amplified stratospheric warm anomaly south of Australia (Figures 9b and 9c).

[31] As the Sun heats the SH during October, the South American anticyclone seen at 20°S in the UTLS intensifies for both EN and LN (Figures 10a and 10b). Strong differences between EN and LN are seen elsewhere at 20°S , with

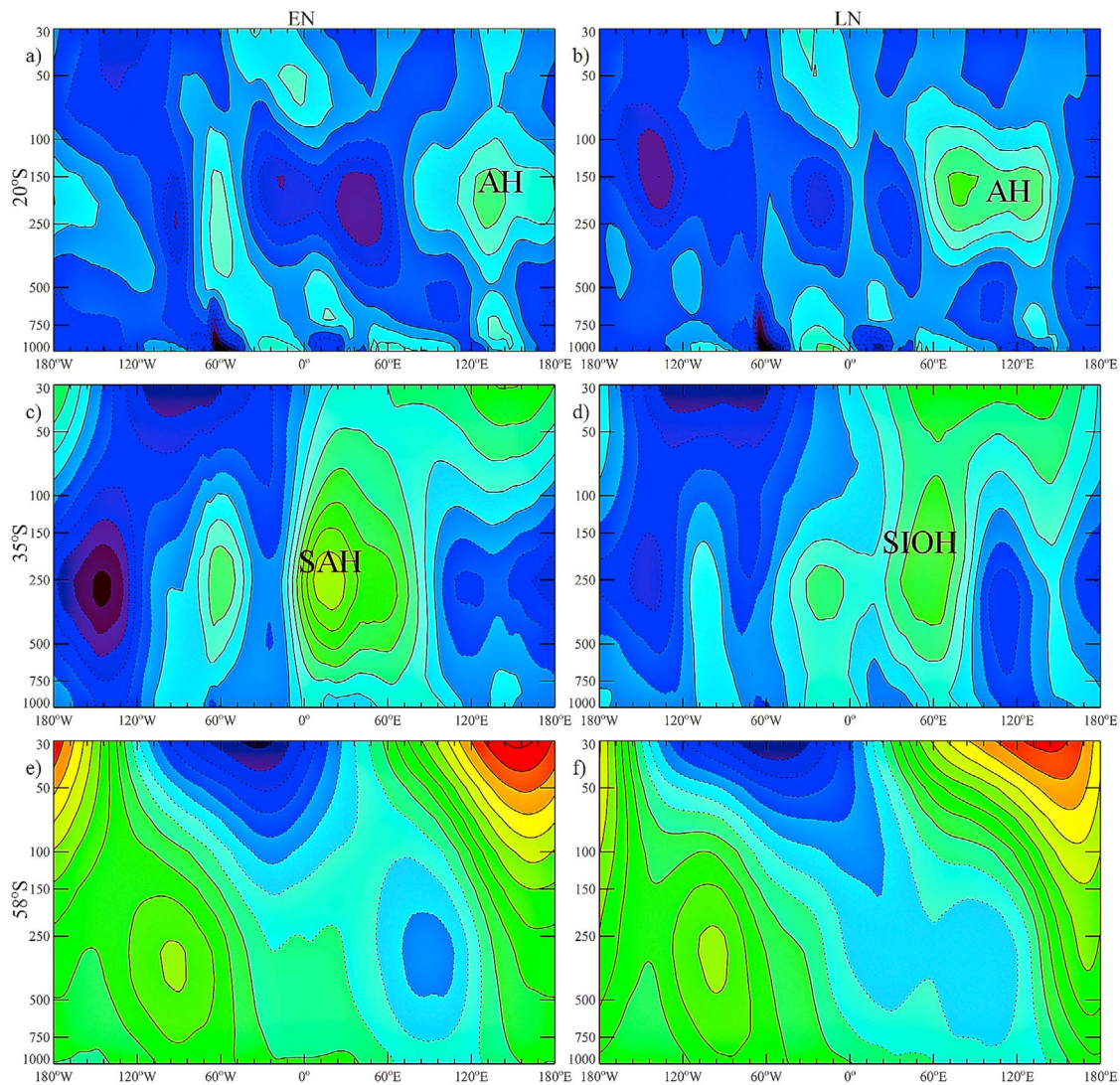


Figure 8. As in Figure 5, except for September. The Australian High (AH), Southern Indian Ocean High (SIOH), and South African High (SAH) are indicated. Note the stronger SAH in Figure 8c and the eastward shift of the wave one pattern at high latitudes during EN.

strong amplification of the Australian High during LN (Figure 10b). At 35°S the SAH is fairly similar for both EN and LN (Figures 10c and 10d), quite different from the very strong SAH during EN in September (Figure 7d). A notable difference between LN and EN at 35°S is the pronounced stratospheric ridge south of the Australian High during LN (Figure 10d). This stratospheric ridge over the Pacific in both EN and LN at 35°S is continuous with the stratospheric ridge in that quadrant at 57.5°S (Figures 10e and 10f). The LN height anomalies at 57.5°S in the lower stratosphere are greater than those of the previous month by 200 gpm and greater than those of EN in October by 200 gpm. The overall structure of the October Antarctic polar vortex during LN is quite robust, coincident with a strong Australian High.

[32] From September to October the thermal anomalies at 20°S are reduced during EN but enhanced during LN. There is a visible westward shift of the LN temperature anomalies in the UTLS at 20°S relative to EN conditions (Figures 11a

and 11b). This is consistent with the intensification and westward shift of the deep thermal anomaly south of Australia during LN (Figure 9). This westward shift and intensification of the warm anomaly near 120°E during LN is also readily apparent at 57.5°S (Figures 11c and 11d) and is intimately related to the LN ozone anomaly in Figure 2i.

5. Dynamical Mechanisms

[33] ENSO differences in column ozone are clearly related to changes in the planetary wave patterns in temperature and geopotential height. In general, energetic tropical convection radiates Rossby wave energy into the midlatitudes [Sardeshmukh and Hoskins, 1988]. Since there are continuous westerlies in the SH lower stratosphere during ASO, the Charney-Drazin criterion allows for propagation of Rossby wave energy associated with subtropical anticyclones in the UTLS to propagate into the extratropical lower stratosphere. This modulates the long-wave patterns

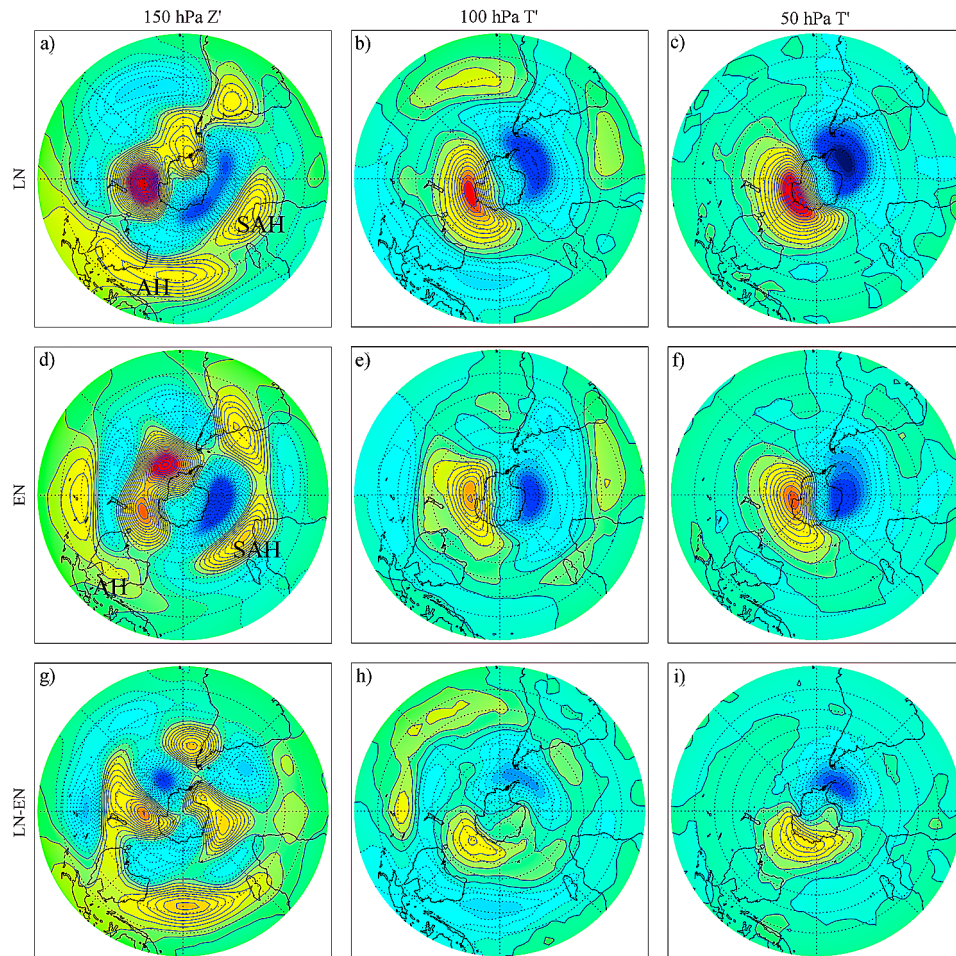


Figure 9. As in Figure 4, except for October. Note the stronger anticyclone near Australia, and the enhanced trough on its poleward flank in Figure 9a overlain by a warm anomaly in Figures 9b and 9c during LN.

of temperature, heights, and ozone. Since ENSO modulates the location of tropical convection, one would expect a modulation of the location of planetary wave structures, as found by previous authors. During each of August, September, and October the tropical and extratropical planetary wave patterns are shifted westward as convection shifts westward during LN, but the detailed mechanism underlying this shift is distinct for each month.

[34] Westward shifts in tropical convection during LN are accompanied by westward shifts in the long-wave patterns for T' and Z' throughout the SH. The antiphased relationship between midtropospheric and lower stratospheric T' anomalies in the tropics is due to the presence or absence of deep convection, where warm tropospheric convection is associated with a higher, colder tropopause and a colder lowest stratosphere. The extension of this pattern to near 20°S may be understood in terms of meridional outflow in the UTLS or the lack of it. Outflow of air with small potential vorticity (PV) from the tropics in the UTLS will create an anticyclone in the subtropics centered near the tropopause. From the point of view of PV thinking [Hoskins *et al.*, 1985], a tropopause level anticyclone, or near-zero PV anomaly, will be underlain by a warm anomaly and

topped by a cold anomaly in the lower stratosphere. Alternatively, an upper tropospheric warm anomaly and lower stratospheric cold anomaly imply the existence of tropopause-centered anticyclonic PV anomaly (J. Egger and K. P. Hoinka, Potential temperature inversion: An alternative to potential vorticity inversion?, submitted to *Journal of Atmospheric Science*).

[35] The antiphased relationship between tropical and extratropical temperature anomalies may be understood as regional meridional circulations. In longitudes with greater deep tropical convection the tropical lower stratosphere will be colder and there will be enhanced poleward outflow from tropical convection about 60° to the west, leading to enhanced subsidence warming in the extratropical lower stratosphere. The angular momentum associated with the tropical outflow creates a longitudinally local jet, with poleward and downward motion causing a warm anomaly on its poleward side. In longitudes with less deep tropical convection, where the tropical lower stratosphere is warmer, there is reduced UTLS outflow and a relative lack of subsidence, hence weaker westerly flow and a cold zonal anomaly in the extratropical lower stratosphere. The relationship between subtropical anticyclones and ozone

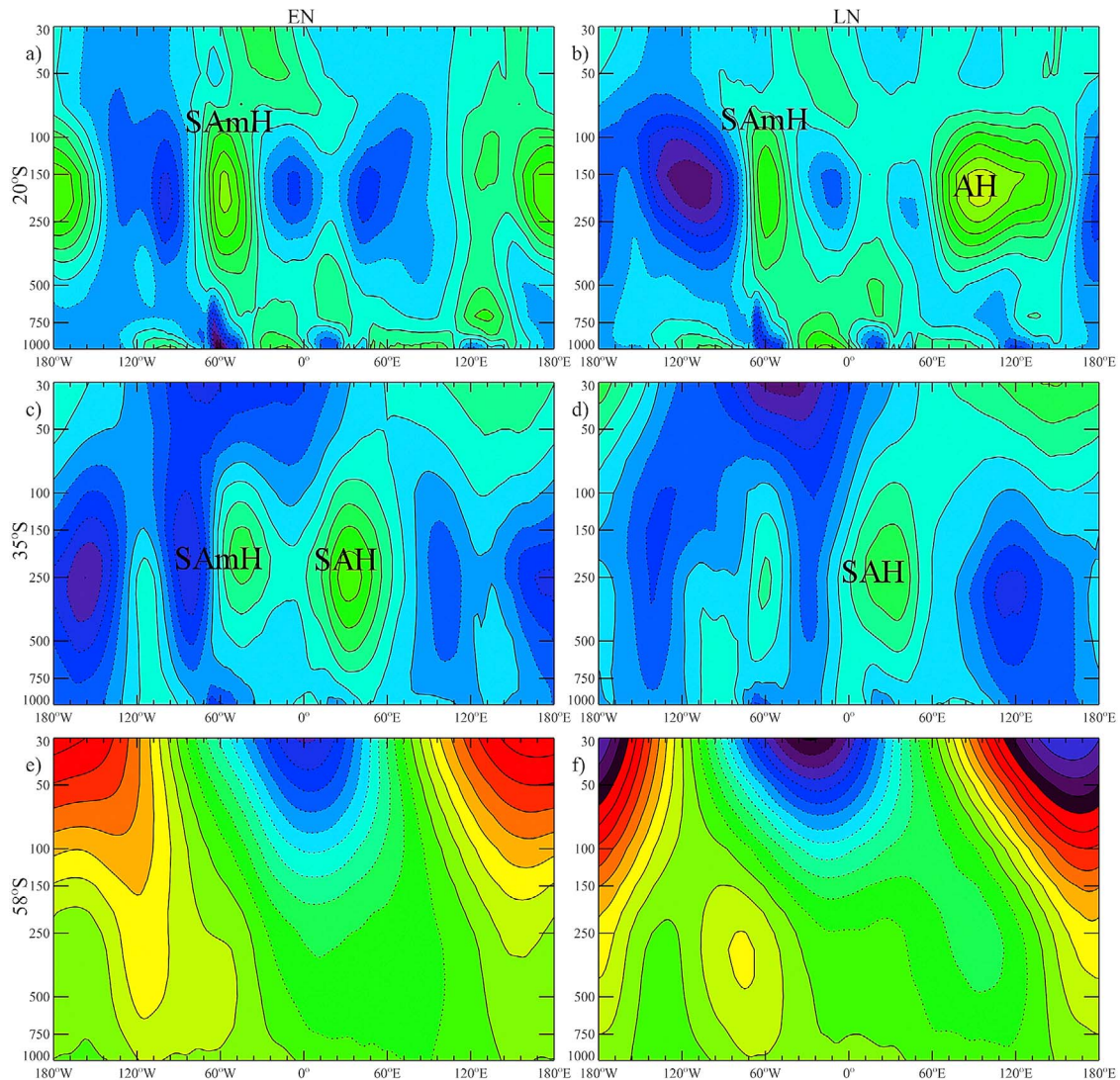


Figure 10. As in Figure 5, except for October. Note the amplified Australian High in Figure 10b and more asymmetric polar vortex in Figure 10f during LN.

anomalies on their poleward flanks is investigated further in the work of Rogal *et al.* [2010].

[36] The relationship between ozone and anticyclones differs between lower stratospheric ridges and UTLS anticyclones, which bears on the mechanisms which cause the LN-EN westward displacement during September and October. During September a distinctive LN-EN warm and positive ozone anomaly near South Africa was shown to be related to the development of a UTLS anticyclone over South Africa during EN. This implies stronger poleward transport of subtropical ozone-poor air near the tropopause level and the divergence of ozone-rich air out of the air column in the lower stratosphere [Koch *et al.*, 2005; Keil *et al.*, 2007; Bian, 2009] during EN. The mean thermal structure shows a cold stratospheric anomaly above a UTLS anticyclone, which is correlated with low ozone. Thus the western end of the ozone croissant is truncated during EN by the presence of this anomalous anticyclone over South Africa.

[37] During October a distinctive LN-EN warm and positive ozone anomaly occurs south of Australia. This

represents an enhancement of the normal wave one warm anomaly present in this region. During LN the UTLS anticyclone over the subtropical Indian Ocean is enhanced when there is more convection over Indonesia (note strong cold region in Figure 3f). This leads to a more intense and zonally confined subtropical westerly jet near Australia during LN. In this longitude band synoptic waves are more effective at transporting ozone and high potential temperature air poleward and downward, yielding the wave one warm, ozone rich ridge that dominates the SH planetary wave pattern in October [Hitchman and Rogal, 2010]. During LN Indonesian convection is enhanced, making the jet stronger, so there is more ozone in the maximum. In addition, the UTLS anticyclone over Australia is stronger during LN. The Australian High interacts with a travelling, ozone-rich, wave-two ridge, which tends to stall and amplify in the Australian sector contributing to the ozone maximum [Hitchman and Rogal, 2010]. Quintanar and Mechoso [1995a, 1995b] showed that stalling and amplification of a wave-two ridge in the Australia-South Pacific sector is quite common

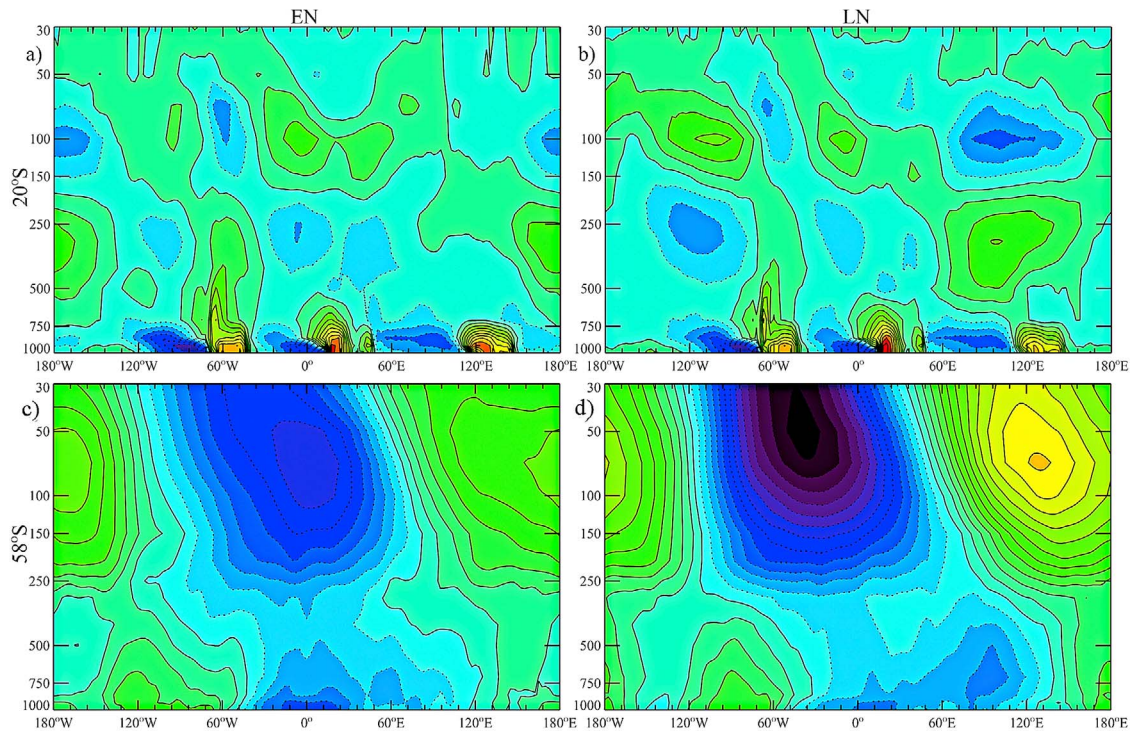


Figure 11. As in Figure 6, except for October. Note the antiphased relationship between the lower stratospheric cold anomaly near 120°E in Figure 11b and the warm ridge in Figure 11f during LN.

during the SH spring. Repeated such events will contribute to a wave-one maximum in monthly mean geopotential height, temperature, and ozone in this sector. During LN convection is focused more intensely over Indonesia during October, enhancing the normal seasonal influence of the Australian High on stalling planetary waves.

6. Conclusions

[38] The analysis presented in this study shows clear differences in general circulation features between EN and LN and the associated modulation of the distribution of column ozone in the SH transition from winter to spring. We have demonstrated that ENSO-induced changes in subtropical anticyclones in the UTLS are distinct during August, September, and October and that there are corresponding, unique changes in the extratropical planetary wave structures which are related to changes in column ozone in the extratropics. There is a strong relationship between barotropic temperature anomalies and column ozone anomalies due to the effects of vertical motion, since both ozone and potential temperature increase upward in the lower stratosphere.

[39] From August to October the ozone maximum intensifies and rotates eastward. For each month this ozone maximum occurs farther west during LN relative to EN, as tropical convection shifts westward in the Pacific basin. Salient ENSO differences include amplification of the UTLS anticyclone off the tip of South Africa during EN and September that diminishes column ozone, and the amplification of the SIO anticyclone during LN and October that

lies immediately equatorward and upstream of the column ozone enhancement.

[40] The September column ozone diminution south of South Africa during EN is related to upward displacement of the tropopause by an anticyclone. But poleward and downward motion of stratospheric air will cause a warm, ozone-rich anticyclone. During October, column ozone enhancement south of Australia during LN is related to an enhanced Australian High and a more zonally focused subtropical westerly jet and enhanced trough on its poleward flank. Poleward and downward motion associated with synoptic waves in the jet creates a region of warm, ozone-rich air in the climatological trough on the poleward side of the jet. The stalling, amplifying wave two ridges in the Pacific sector contribute to the monthly mean wave-one, warm ozone-rich maximum in the base of the wave one ridge.

[41] **Acknowledgments.** This work was supported by NSF grant ATM-0822858 and NASA grant NNX08AW52G.

References

- Angell, J. K. (1992), Evidence of a relation between El Niño and QBO, and for an El Niño in 1991–92, *Geophys. Res. Lett.*, *19*(3), 285–288, doi:10.1029/91GL02731.
- Baldwin, M. P., and T. J. Dunkerton (1998), Quasi-biennial modulation of the Southern Hemisphere stratospheric polar vortex, *Geophys. Res. Lett.*, *25*, 3343–3346.
- Berbery, H., and C. Vera (1996), Characteristics of the southern hemisphere winter storm track with filtered and unfiltered data, *J. Atmos. Sci.*, *53*, 468–481.
- Bian, J. (2009), Features of ozone mini-hole events over the Tibetan Plateau, *Adv. Atmos. Sci.*, *26*, 305–311.

- Bojkov, R. D. (1987), The 1983 and 1985 anomalies in ozone distribution in perspective, *Mon. Weather Rev.*, *115*, 2187–2201.
- Bowman, K. P. (1989), Global patterns of the quasi-biennial oscillation in total ozone, *J. Atmos. Sci.*, *46*, 3328–3343.
- García-Herrera, R., N. Calvo, R. R. García, and M. A. Giorgetta (2006), Propagation of ENSO temperature signals into the middle atmosphere: A comparison of two general circulation models and ERA-40 reanalysis data, *J. Geophys. Res.*, *111*, D06101, doi:10.1029/2005JD006061.
- Garfinkel, C. I., and D. L. Hartmann (2007), Effects of the El-Niño Southern Oscillation and the quasi-biennial oscillation on polar temperatures in the stratosphere, *J. Geophys. Res.*, *112*, D19112, doi:10.1029/2007JD008481.
- Hamilton, K. (1993), An examination of observed Southern Oscillation effects in the Northern Hemisphere stratosphere, *J. Atmos. Sci.*, *50*, 3468–3473.
- Hampson, J., and P. Haynes (2006), Influence of the equatorial QBO on the extratropical stratosphere, *J. Atmos. Sci.*, *63*, 936–951.
- Hasebe, F. (1980), A global analysis of the fluctuations in total ozone, II, Non-stationary annual oscillation, quasi-biennial oscillation, and long-term variations in total ozone, *J. Meteorol. Soc. Jpn.*, *58*, 104–117.
- Hastenrath, S. (1990), The relationship of highly reflective clouds to tropical climate anomalies, *J. Clim.*, *3*, 353–365.
- Hio, Y., and I. Hirota (2002), Interannual variation of planetary waves in the Southern Hemisphere stratosphere, *J. Meteorol. Soc. Jpn.*, *80*, 1013–1027.
- Hitchman, M. H., and A. S. Huesmann (2009), Effect of the Quasi-biennial Oscillation on stratospheric jets and Rossby wave breaking, *J. Atmos. Sci.*, *66*, 935–946.
- Hitchman, M. H., and M. J. Rogal (2010), Influence of tropical convection on the Southern Hemisphere ozone maximum during the winter to spring transition, *J. Geophys. Res.*, *115*, D14118, doi:10.1029/2009JD012883.
- Hollingsworth, A., D. B. Shaw, P. Lonnberg, L. Illari, K. Arpe, and A. J. Simmons (1986), Monitoring of observation and analysis quality by a data assimilation system, *Mon. Weather Rev.*, *114*, 861–879.
- Hood, L., S. Rossi, and M. Beuten (1999), Trends in lower stratospheric zonal winds, Rossby wave breaking behavior, and column ozone at northern midlatitudes, *J. Geophys. Res.*, *104*, 24,321–24,339.
- Hoskins, B. J., M. E. McIntyre, and A. W. Robertson (1985), On the use and significance of isentropic potential vorticity maps, *Q. J. R. Meteorol. Soc.*, *111*, 877–946.
- Hudson, R. D., A. D. Frolov, M. F. Andrade, and M. B. Follette (2003), The total ozone field separated into meteorological regimes, Part I: Defining the regimes, *J. Atmos. Sci.*, *60*, 1669–1677.
- Hudson, R. D., M. F. Andrade, M. B. Follette, and A. D. Frolov (2006), The total ozone field separated into meteorological regimes - Part II: Northern Hemisphere mid-latitude total ozone trends, *Atmos. Chem. Phys.*, *6*, 5183–5191.
- Kallberg, P., et al. (2005), ECMWF Re-Analysis Project Report Series, 19, 191 pp.
- Keil, M., D. R. Jackson, and M. C. Hort (2007), The January 2006 low ozone event over the UK, *Atmos. Chem. Phys.*, *7*, 961–972.
- Koch, G., et al. (2005), A composite study on the structure and formation of ozone miniholes and minihighs over central Europe, *Geophys. Res. Lett.*, *32*, L12810, doi:10.1029/2004GL022062.
- Kayano, M. T. (1997), Principal modes of the total ozone on the Southern Oscillation time scale and related temperature variations, *J. Geophys. Res.*, *102*, 25,797–25,806.
- Kinnersley, J. S., and K. K. Tung (1998), Modeling the global interannual variability of the ozone column due to the equatorial quasi-biennial oscillation and extratropical planetary wave variability, *J. Atmos. Sci.*, *55*, 1417–1428.
- Kinnersley, J. S., and K. K. Tung (1999), Mechanisms for the extra-tropical QBO in circulation and ozone column, *J. Atmos. Sci.*, *56*, 1942–1962.
- Labitzke, K., and H. van Loon (1992), On the association between the QBO and the extratropical stratosphere, *J. Atmos. Terr. Phys.*, *54*, 1453–1463.
- McCormack, J. P., and L. L. Hood (1994), Relationship between ozone and temperature trends in the lower stratosphere: Latitude and seasonal dependences, *Geophys. Res. Lett.*, *21*, 1615–1618.
- Newman, P. A., and W. J. Randel (1988), Coherent ozone-dynamical changes during the Southern Hemisphere spring, 1979–1986, *J. Geophys. Res.*, *93*, 12,585–12,606.
- Pascoe, C. L., L. J. Gray, S. A. Crooks, M. N. Jukes, and M. P. Baldwin (2005), The quasi-biennial oscillation: Analysis using ERA-40 data, *J. Geophys. Res.*, *110*, D08105, doi:10.1029/2004JD004941.
- Perliski, L. M., S. Solomon, and J. London (1989), On the interpretation of seasonal variations of stratospheric ozone, *Planet. Space Sci.*, *37*, 1527–1538.
- Quintanar, A. I., and C. R. Mechoso (1995a), Quasi-stationary waves in the Southern Hemisphere, Part I: Observational Data, *J. Clim.*, *8*, 2659–2672.
- Quintanar, A. I., and C. R. Mechoso (1995b), Quasi-stationary waves in the Southern Hemisphere, Part II: Generation mechanisms, *J. Clim.*, *8*, 2673–2690.
- Randel, W. J., and J. B. Cobb (1994), Coherent variations of monthly mean total ozone and lower stratospheric temperature, *J. Geophys. Res.*, *99*, 5433–5477.
- Randel, W. J., F. Wu, and R. Stolarski (2002), Changes in column ozone correlated with the stratospheric EP flux, *J. Meteorol. Soc. Jpn.*, *80*, 849–862.
- Rogal, M. J., M. H. Hitchman, M. L. Buker, G. J. Tripoli, I. Stajner, and H. Hayashi (2010), Modeling the effects of Southeast Asian monsoon outflow on subtropical anticyclones and midlatitude ozone over the Southern Indian Ocean, *J. Geophys. Res.*, doi:10.1029/2009JD012979, in press.
- Sardeshmukh, P. D., and B. J. Hoskins (1988), The generation of global rotational flow by steady idealized tropical divergence, *J. Atmos. Sci.*, *45*, 1228–1251.
- Sassi, F., D. Kinnison, B. A. Bouville, R. R. Garcia, and R. Roble (2004), Effect of El Niño-Southern Oscillation on the dynamical, thermal, and chemical structure of the middle atmosphere, *J. Geophys. Res.*, *109*, D17108, doi:10.1029/2003JD004434.
- Schubert, S. D., and M. J. Munteanu (1988), An analysis of tropopause pressure and total ozone correlations, *Mon. Weather Rev.*, *116*, 569–582.
- Shiotani, M. (1992), Annual, quasi-biennial, and El Niño - Southern Oscillation (ENSO) time-scale variations in equatorial total ozone, *J. Geophys. Res.*, *97*, 7625–7633.
- Steinbrecht, W., H. Claude, U. Kohler, and K. P. Hoinka (1998), Correlations between tropopause height and total ozone: Implications for long-term changes, *J. Geophys. Res.*, *103*, 19,183–19,192.
- Stolarski, R. S., M. R. Schoeberl, P. A. Newman, R. D. McPeters, and A. J. Krueger (1990), The 1989 Antarctic ozone hole as observed by TOMS, *Geophys. Res. Lett.*, *17*, 1267–1270.
- Stolarski, R. S., P. Bloomfield, R. D. McPeters, and J. R. Herman (1991), Total ozone trends deduced from Nimbus 7 TOMS data, *Geophys. Res. Lett.*, *18*, 1015–1018.
- Trenberth, K. (1992), Global analyses from ECMWF and atlas of 1000 to 10 mb circulation statistics, *NCAR/TN-373+STR*, 205 pp., Natl. Cent. for Atmos. Res., Boulder, Colo.
- van Loon, H., and K. Labitzke (1987), The Southern Oscillation, Part V: The anomalies in the lower stratosphere of the Northern Hemisphere in winter and a comparison with the Quasi-Biennial Oscillation, *Mon. Weather Rev.*, *115*, 357–369.
- van Loon, H., C. S. Zerefos, and C. C. Repapis (1982), The Southern Oscillation in the stratosphere, *Mon. Weather Rev.*, *110*, 225–229.
- Wirth, V. (1991), What causes the seasonal cycle of stationary planetary waves in the southern stratosphere?, *J. Atmos. Sci.*, *48*, 1194–1200.
- Wirth, V. (1993), Quasi-stationary planetary waves in total ozone and their correlation with lower stratospheric temperature, *J. Geophys. Res.*, *98*, 8873–8882.

M. H. Hitchman and M. J. Rogal, Department of Atmospheric and Oceanic Sciences, University of Wisconsin–Madison, 1225 West Dayton Street, Madison, WI 53706, USA. (matt@aos.wisc.edu)